Simple potential model for cluster states in light nuclei*

B. Buck†
Department of Theoretical Physics, Oxford University, 12 Parks Road, Oxford, England

C. B. Dover and J. P. Vary
Brookhaven National Laboratory, Upton, New York 11973

(Received 14 January 1975)

We present a simple model for three and four particle cluster states in light nuclei. These states are considered as bound states and single particle resonances of a cluster-core potential, which is obtained by folding the cluster and core mass densities. We calculate some properties of these states in ^{16}O and ^{20}Ne, such as the rms radii, $B(E2)$ values, α-decay widths, and energy spectra. Good agreement with available data is obtained and some predictions are made for $B(E2)$ values in the $K^\pi = 0^-$ bands in ^{16}O and ^{20}Ne. This model is also used to interpret recent heavy ion three particle transfer data. Dynamical support is offered for high spin assignments in ^{15}N and ^{15}O previously based on kinematical considerations.

[NUCLEAR STRUCTURE ^{15}N, ^{16}O, ^{20}Ne; calculated energies, J, π, $B(E2)$ values, α widths, radii in cluster model with folded potential.]

I. INTRODUCTION

The principal motivation for the present work stems from a desire to interpret in a simple and intuitive way several striking features of nuclear reactions involving three and four particle transfer, namely:

(a) the strong selectivity in reactions such as ^{12}C(^{10}B, ^{7}Be)^{15}N,[1] for example, over and above the L transfer and Q-value dependence. Such data have been interpreted[2] in terms of direct three nucleon transfer populating *high-spin* states.

(b) in four particle transfer reactions such as (^{6}Li, d), (^{7}Li, t), and (^{16}O, ^{12}C) on light targets such as ^{12}C and ^{16}O, several well-known rotational bands in ^{16}O and ^{20}Ne are preferentially populated. Such observations, plus the fact that the α-decay widths of certain of these levels are rather close to the single particle Wigner limit, have been interpreted in terms of a direct α-cluster transfer mechanism.[3-6]

We propose to correlate our understanding of such experimental results and their corresponding implications for nuclear structure by introducing a simple cluster description of that restricted class of nuclear states which are strongly populated in multiparticle transfer reactions of the above type or which have characteristically large widths. We deliberately confine our attention to this rather narrow class of states, for which the concept of "cluster structure" may have at least some qualitative usefulness.

The model, in the form we adopt, provides a convenient framework for making predictions of the energies of high-spin states. We would like to provide dynamical support for spin assignments of certain states, which have been based thus far on the purely kinematical Brink selection rules.[7,8] It should be emphasized, however, that the simple cluster model is not designed to replace the more detailed predictions of the nuclear shell model. Indeed, there is known to be a large degree of overlap between shell-model wave functions for members of certain rotational bands in light nuclei and wave functions generated by less general models such as the Bloch-Brink cluster model[9] and the SU(3) model.[10,11] The advantage of our simple model, which neglects exchange effects, is the relative ease with which a wide variety of calculations may be performed, including cases for which the full shell-model basis of states would be very large. All cluster models represent a choice of a small set of states to replace the much larger shell-model basis and so their usefulness is restricted to nuclear states of a particularly simple structure. The goal of this paper is to show that a simple cluster picture accounts rather well for the properties of such states.

In this model, we search for the bound states and single particle resonances of a cluster-core potential which is approximated by a folding of the cluster density $\rho_A(r)$ with the core density $\rho_B(r)$

$$V(r) = -\frac{2\pi\hbar^2}{M}\bar{f}\int d\vec{r}'\,\rho_A(\vec{r}-\vec{r}')\rho_B(\vec{r}')\,, \qquad (1.1)$$

where M is the nucleon mass and $\bar{f}$ is a depth parameter, here taken to be real; the densities $\rho_A(r)$ and $\rho_B(r)$ are taken from electron scattering analyses.[12] In writing Eq. (1.1), we have made

several assumptions which may be only qualitatively valid; for example (a) we assume that the correlations of the particles in a cluster embedded in the nucleus are the same as those of a cluster in free space; (b) we ignore exchange effects between the particles in the cluster and those in the core; (c) the nucleon-nucleon interaction has zero range.

In order to show that these approximations are reasonable, we check the consistency of a variety of calculated properties; (a) rms radius of the composite system; (b) energy separation between members of a band; (c) $B(E2)$ values for electromagnetic transitions between members of a band calculated as single particle transitions; (d) α widths of continuum states; (e) localization of cluster wave functions outside the radius of the core. If we have such localization, we are perhaps justified *a posteriori* in neglecting exchange effects between cluster and core. The blocking effects of the Pauli principle, which prevent nucleons of the cluster from entering single particle states already occupied by core nucleons, are well approximated by means of a careful choice of the quantum numbers of bound states of the cluster relative to the core. This choice is indicated below.

A simple folding model given in Eq. (1.1) has also proved useful in a variety of other situations, such as α-particle elastic and inelastic scattering,[13,14] and heavy ion elastic scattering and one and two particle transfer reactions.[13] Part of the motivation for the present study was to test the applicability of the folding model for composite systems in yet another context. A detailed discussion of the folding model and its limitations is given by Dover and Vary.[15]

II. FOLDED POTENTIAL

In the present study, we adopt the most extreme form of the cluster model, in which the cluster is viewed as a single particle in a certain orbit with principal quantum number N and orbital quantum number L, circulating around an inert core. The values of N and L are related to the n_i and l_i of the particles which make up the cluster in the usual way[16]:

$$2N+L=\sum_{i=1}^{n_c}(2n_i+l_i)\,, \tag{2.1}$$

where n_c is the number of particles in the cluster. Note that the values n_i and l_i correspond to the filling of the shell-model orbitals *above* the closed core. For ^{20}Ne considered as $^{16}\mathrm{O}+\alpha$, for example, the lowest-lying states considered here correspond to dropping the four particles into the $2s$-$1d$ shell

TABLE I. Parameters for a modified Gaussian density.

Nucleus	α	R (fm)
^{3}H	0	1.64
^{3}He	0	1.77
^{12}C	1.33	2.47
^{16}O	1.60	2.75

$(2n_i+l_i=2)$ rather than the $1s$ or $1p$ shell. Thus we satisfy the most obvious requirement of the Pauli principle by hand.

Our procedure is then to solve a one particle Schrödinger equation for a state specified by N and L, with a single particle potential of the form

$$V_{\mathrm{opt}}(r)=V(r)+V_{\mathrm{so}}(r)\,, \tag{2.2}$$

where the central potential $V(r)$ is given by

$$V(r)=-\frac{2\pi\hbar^2}{M}\bar{f}\int d^3\vec{r}\,'\rho_A(\vec{r}-\vec{r}\,')\rho_B(\vec{r}\,') \tag{2.3}$$

and the cluster spin-orbit potential $V_{\mathrm{so}}(r)$ is assumed to be

$$V_{\mathrm{so}}(r)=-V_{\mathrm{so}}\left(\frac{\hbar}{m_\pi c}\right)^2\frac{1}{r}\left|\frac{dV(r)}{dr}\right|\vec{l}\cdot\vec{\sigma}\,, \tag{2.4}$$

where $(\hbar/m_\pi c)^2=2$ fm^2 and $\vec{\sigma}$ is the spin of the cluster (eigenvalues $\sigma_z=\pm1$ for spin $\frac{1}{2}$). The strength constants $\bar{f}$ and V_{so} are regarded as adjustable real constants; they are allowed to depend on the band under consideration (the $2N+L$ value), but *not* on the particular state within a band. In other applications[13,15] $\bar{f}$ is related to the effective nucleon-nucleon scattering amplitude in the medium. Thus we are dealing with a *local* energy independent potential for each band. This is in contrast to treatments using Woods-Saxon potentials,[17-19] for which a different depth is required to fit the energy of each state. In addition to the nuclear potential of Eq. (2.2), we have added the Coulomb potential of a uniform spherical charge distribution of radius 3.5 fm for $\alpha+^{12}$C and 3.53 fm for $\alpha+^{16}$O.

For the densities $\rho_{A,B}(r)$ of cluster and core, we have used parametrized forms obtained from electron scattering analyses[12] and have assumed that the neutron and proton densities have the same radial shape. For ^{3}H, ^{3}He, ^{12}C, and ^{16}O, we use modified Gaussian densities of the form

$$\rho(r)=C(1+\alpha\gamma^2y^2)e^{-\gamma^2y^2}\,, \tag{2.5}$$

where $y=r/R$, R being the rms radius, $\gamma=[3(2+5\alpha)/2(2+3\alpha)]^{1/2}$, and C is a normalization constant adjusted so that $\int d^3\vec{r}\rho(r)$ yields the number of particles. The parameters α and R are listed

in Table I. For the α particle, we have used a three parameter Fermi distribution

$$\rho(r)=\rho_0(1+wr^2/c^2)\Big/\left[1+\exp\left(\frac{r-c}{a}\right)\right] \tag{2.6}$$

with $c=1.01$ fm, $a=0.372$ fm, and $w=0.445$[12]; which yields an rms radius of 1.71 fm. It is also possible to use the modified Gaussian form (2.5), or even a simple Gaussian function, for the α-particle density. The results we obtain are nearly independent of the exact choice of density function providing the parameters are consistent with the measured rms radius. These alternative forms have the advantage that the folding integral of Eq. (2.3) may be calculated analytically; in this paper, we use Eq. (2.6) for the α density, however. The assumption that the mass density follows the charge density seems sufficient for the present qualitative level of our discussion. The influence of the details of the densities $\rho(r)$ (i.e., the behavior of the tail region) on the structure of $V_{\rm opt}(r)$ is discussed in Ref. 15.

We illustrate in Fig. 1 how the folded potential compares with conventional Woods-Saxon potentials. We have chosen the case of $\alpha+{}^{16}$O, with the value of $\bar{f}=1.237$ fm chosen to give the correct absolute energy for the 2^+ member of the ground state band in ^{20}Ne. The Woods-Saxon potentials shown are of the form

$$V_{\rm WS}(r)=\frac{-V_0}{1+\exp\left(\frac{r-R}{a}\right)} \tag{2.7}$$

with $R=3.53$ fm and $a=0.6$ fm. The depths are $V_0=114.78$, 111.47, 106.56, 94.95, and 89.71, respectively, for the 0^+, 2^+, 4^+, 6^+, and 8^+ members of the ^{20}Ne ground state band. The depths V_0 must be adjusted separately for each state in order to obtain the correct energy. A Woods-Saxon potential of this geometry with a fixed value of V_0 gives essentially a degenerate or inverted spectrum. The crucial geometrical property of the folded potential, which enables one to obtain a

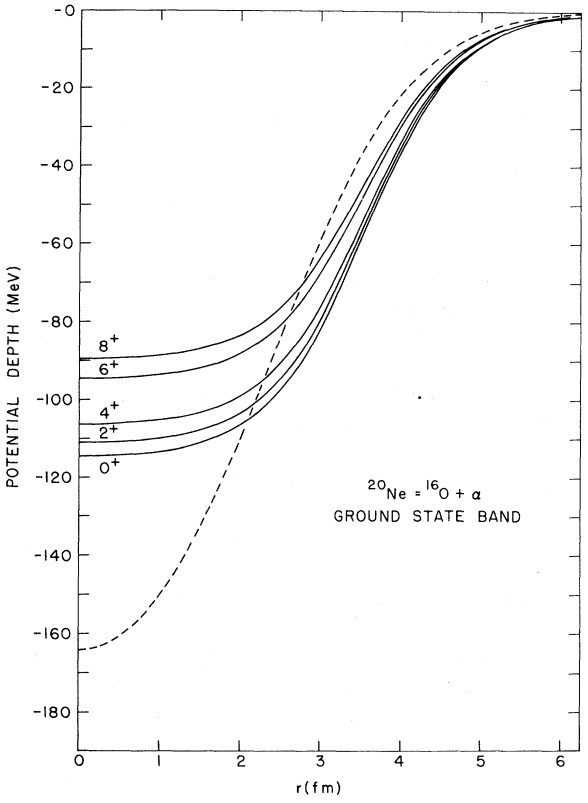

FIG. 1. Single particle potentials appropriate to the ground state band of ^{20}Ne, viewed as $\alpha+{}^{16}$O. The solid curves are Woods-Saxon potentials of Eq. (2.7) whose depth V_0 was adjusted separately for each state 0^+, 2^+, 4^+, 6^+, and 8^+ in order to fit the experimental binding energy; we have $V_0=114.78$, 111.47, 106.56, 94.95, and 89.71 MeV, respectively (Ref. 18). A radius $R=3.53$ fm and a diffuseness $a=0.6$ fm were used for each state. The dashed curve represents the folded potential of Eq. (2.3) with $\bar{f}=1.237$ fm which produces the spectrum shown in Fig. 5.

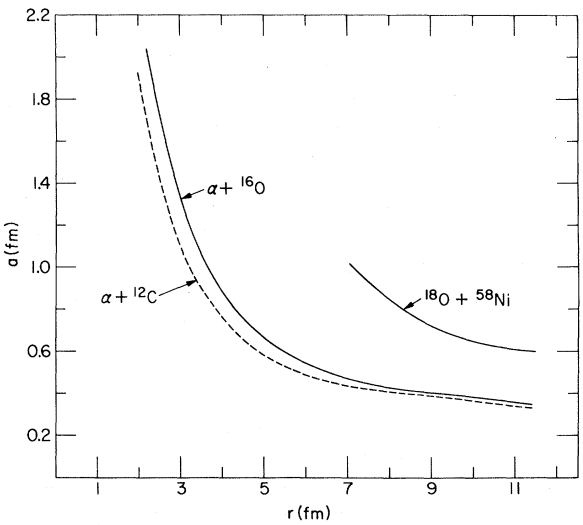

FIG. 2. Equivalent diffuseness a of the folded potential Eq. (2.3), obtained by matching an exponential tail $C\exp(-r/a)$ to the folded form at each value of r. The $\alpha+{}^{12}$C and $\alpha+{}^{16}$O curves correspond to the density parameters below Eq. (2.6) for the α particle and the parameters of Table I for ^{12}C and ^{16}O. A typical curve for a heavy ion situation (^{18}O+^{58}Ni) is also shown; in this case the densities were taken from a single particle model (Ref. 15). Note that a is quite large (~ 1 fm) in the region $r\approx 3-4$ fm where the α cluster is localized. For the ^{18}O+^{58}Ni case, on the other hand, we obtain the more conventional value (Ref. 58) $a\approx 0.65$ fm at the critical radius (Ref. 58) $r\approx 10$ fm for low energy elastic scattering (2–10 MeV/particle).

spectrum exhibiting the correct energy splitting with a *single* value of $\bar{f}$ per band, is shown in Fig. 2. In this figure, we plot the effective diffuseness a obtained by fitting an exponential tail $-V_0 e^{R/a} e^{-r/a}$ to the calculated folded potential. The point to note is that the effective diffuseness is quite *large* for radii where the main cluster probability is concentrated (see Figs. 8 and 9 in Sec. III). Since the energy splitting of states of different spin is sensitive to the diffuseness, the success of the folded potential in reproducing roughly the correct splittings can be mainly attributed to the large effective diffuseness. In Fig. 2, we also show the effective diffuseness for a typical heavy ion situation, $^{18}O + ^{58}Ni$. In this case, the diffuseness in the region of $r \approx 10$ fm, corresponding to a grazing collision, is close to the more conventional value $a = 0.65$ fm.

III. α-CLUSTER STATES IN LIGHT NUCLEI

Before proceeding to the more speculative calculations involving three particle clusters, we first investigate several well established rotational bands in light nuclei, which are thought to possess a relatively high degree of α-cluster structure.[5,16,20-23] These well-known cases serve as a testing ground, in order to ascertain whether the folded model is likely to have any useful predictive power in the more interesting cases where the spins and energies of the states in question are unknown. These calculations provide a much simpler description of the rotational bands than the detailed dynamical calculations which have been performed.[24-26]

The bands we shall discuss are the following:

(a) $2N + L = 8$, corresponding to the shell-model approximation of four particles in the $2s$-$1d$ shell. This gives a $K^\pi = 0^+$ band with spins 0^+, 2^+, 4^+, 6^+, 8^+, corresponding to $N = 4, 3, 2, 1, 0$, respectively. We identify these states with the ground state rotational band in ^{20}Ne and the band in ^{16}O based on the 6.06 MeV 0^+ excited state.[19,27]

(b) $2N + L = 9$, corresponding to three $2s$-$1d$ particles and one $1f$-$2p$ particle. This gives a $K^\pi = 0^-$ band with spins 1^-, 3^-, 5^-, 7^-, 9^-. We take this band to correspond to rotational bands in ^{16}O and ^{20}Ne based on 1^- states at 9.58 and 5.79 MeV, respectively.[19,27] Note that for the first $K^\pi = 0^-$ band in ^{16}O, a $2N + L = 7$ cluster assignment is not yet excluded by the data, since the 9^- member of the band has not yet been observed experimentally.[19] However, the latter assignment would require one nucleon of the α cluster to be in the $1p$ shell, which is largely blocked.

Before proceeding with a discussion of the cluster results, it is useful to establish a perspective by considering briefly other models. This will serve to emphasize the high degree of overlap between the various models and to pinpoint those features of the data which are relatively hard to explain theoretically.

A variety of models have been invoked to describe rotational bands in light nuclei: (a) the full shell model[24,25,56]; (b) the SU(3) model[10,11]; (c) the Bloch-Brink cluster model[9,16]; (d) deformed oscillator model[22]; (e) Hartree-Fock method[26,28,29]; (f) generator coordinate method[30]; (g) resonating group method.[54,55] We will not discuss all of these in detail; instead we concentrate on elucidating the differences and similarities between (a)–(c). Note, however, that our treatment is similar to the resonating group method (g), except that we use a different effective potential and take account of the orthogonality condition[54,55] approximately by our choice of quantum numbers for cluster-core states.

Full shell-model calculations for ^{20}Ne and ^{16}O have been performed by several authors.[16,24,25,56] Here one assumes a single particle Hamiltonian H_0 which generates a basis of states. Then one diagonalizes a residual nucleon-nucleon interaction within this basis. Such calculations treat the interacting system of four $2s$-$1d$ (or $2s$-$1d$-$1p$) particles outside an inert ^{16}O (or ^{12}C) core. The shell-model diagonalization produces in general a large number of states. Certain of these states, however, exhibit a very large degree of overlap with simple SU(3) model wave functions.[24,31] In the SU(3) description, the ground state band of ^{20}Ne, for example, corresponds mainly to the $[f](\lambda\mu) = [4](80)$ representation of SU(3). The $K^\pi = 0^-$ excited band corresponds to the [4](90) representation of SU(3). The overlap of the complete shell-model wave functions and the SU(3) [4](80) wave functions is of order 89.5, 90.6, 84.8, 87.5, and 80.6 (in percent) for the ^{20}Ne ground state band.[24] These results indicate that the SU(3) model represents a judicious choice of basis for a certain restricted class of nuclear states. It is well known[32] that the SU(3) model and an *antisymmetrized* form of the cluster model are fully equivalent. For ^{20}Ne, this form of the cluster model yields a wave function of the form

$$\psi_{LM}(^{20}\mathrm{Ne}) = N\mathcal{A}\phi_0(^{16}\mathrm{O})\phi_0(\alpha)u_{NLM}(r)\Phi_{\mathrm{c.m.}}\,, \qquad (3.1)$$

where ϕ_0 is an intrinsic oscillator wave function for ^{16}O or α, taken as the lowest state of an harmonic oscillator (same oscillator parameter for α and ^{16}O), $u_{NLM}(r)$ is a wave function for the relative motion of the α-^{16}O system [N and L must be chosen according to Eq. (2.1)], $\Phi_{\mathrm{c.m.}}$ is a center of mass wave function, and $\mathcal{A}$ is an anti-

symmetrizer which enforces the requirements of the Pauli principle. The cluster model wave functions of Eq. (3.1) and the shell-model wave functions have a very large degree of overlap for the rotational bands under discussion here.

One of the signatures for the α-cluster structure of a state is its α-decay width Γ_L. In the framework of R-matrix theory, we have[19]

$$\Gamma_L = 2P_L(a)\gamma_L^2(a) , \tag{3.2}$$

where $P_L(a)$ is the penetrability and $\gamma_L^2(a)$ is the reduced width given by

$$P_L(a) = ka[F_L^2(ka) + G_L^2(ka)]^{-1} ,$$
$$\gamma_L^2(a) = \theta_L^2(a)\gamma_W^2(a) . \tag{3.3}$$

In Eq. (3.3), F_L and G_L are regular and irregular Coulomb wave functions and the single particle Wigner limit $\gamma_W^2(a) = 3\hbar^2/2\mu a^2$, where μ is the reduced mass and a is the channel radius.[33] Qualitatively, a large value of $\theta_L^2 \approx 1$ can be taken as evidence to support a cluster interpretation of a state. For instance, in Ref. 22, values $\theta_L^2 = (>0.54)$, 0.89, 1.06, 0.79 are given for the 1^-, 3^-, 5^-, and 7^- states of the $K^\pi = 0^-$ band in ^{20}Ne, using Eqs. (3.2) and (3.3) with a channel radius $a = 5$ fm. This band is thus a prime candidate for a cluster interpretation.[20-22]

It is important to see to what extent the simple SU(3) or cluster models can account for the observed α widths. Several extensive studies of this question have been made.[17-19,22,34] Such analyses are usually expressed in terms of a reduced width amplitude $\mathcal{Y}_L(r)$ defined by

$$\mathcal{Y}_L(r) = \binom{20}{4}^{1/2} \langle Y_{L0}\phi_0(\alpha)\phi_0(^{16}\mathrm{O})|\psi_{L0}(^{20}\mathrm{Ne})\rangle \tag{3.4}$$

for the example of ^{20}Ne, where ψ_{L0} is given by Eq. (3.1) for the SU(3) or cluster model. The reduced width $\gamma_L(a)$ is related to $\mathcal{Y}_L(r)$ evaluated at the channel radius a

$$\gamma_L(a) = \left(\frac{\hbar^2 a}{2\mu}\right)^{1/2} \mathcal{Y}_L(r)\Big|_{r=a} . \tag{3.5}$$

The function $\mathcal{Y}_L(r)$ may be thought of roughly as the radial wave function for the α cluster, except that its over-all normalization is affected by the presence of the antisymmetrizer $\mathcal{A}$ in Eq. (3.1). We have

$$\int_0^\infty \mathcal{Y}_L^2(r) r^2 dr = S_L , \tag{3.6}$$

where S_L is a spectroscopic factor between 0 and 1. For a pure SU(3) representation, S_L can be evaluated analytically[22]; we get $S_L = 0.23$ and 0.344 for states of the [80] and [90] bands, respectively. The naive cluster picture yields of course $S_L = 1$. Thus we see that antisymmetry is very important for SU(3) wave functions. However, the fact that S_L is small for SU(3) wave functions leads to predicted α widths which are also too small.[22] For instance, values $\theta_L^2 = 0.1$, 0.09, 0.07, and 0.04 were obtained in Ref. 22 for the 1^-, 3^-, 5^-, and 7^- members, respectively, of the $K^\pi = 0^-$ band in ^{20}Ne, treating this band as a pure SU(3) [4](90) configuration. These are to be compared with experimental values of the order of 0.8–1.0.[22,27] Thus, in Ref. 22, there is an order of magnitude discrepancy between the SU(3) widths and experiment.

Much of this width discrepancy disappears if one employs a Bloch-Brink cluster wave function[9,22] of the type

$$\psi_L(^{20}\mathrm{Ne}) = N_L P_{L0}\mathcal{A}[\phi_0(\alpha, R_A, \nu_A)\phi_0(^{16}\mathrm{O}, R_B, \nu_B)] , \tag{3.7}$$

where $\phi_0(\alpha, R_A, \nu_A)$ is an harmonic oscillator wave function centered at R_A with oscillator parameter ν_A, and P_{L0} is an angular momentum projection operator. In general $\nu_A \neq \nu_B$; for $\nu_A = \nu_B$, we have $R_A = 4/5R$, $R_B = -1/5R$ so that $R_A - R_B = R$ = relative separation of α and ^{16}O. With the wave function of Eq. (3.7), Horiuchi and Suzuki[22] obtain values $\theta_L^2 \approx 0.56$ for the $K^\pi = 0^-$ band in ^{20}Ne, from a factor 6 to more than an order of magnitude larger than the SU(3) prediction, and in better agreement with experiment. The reason for this relative success is illustrated in Fig. 3, where we plot the radial function $r\mathcal{Y}_L(r)$ for the 1^- member of the band. The SU(3) wave function is seen to have a considerable overlap with the nuclear interior, i.e., the α cluster has a sizable probability of sitting inside the core radius, and hence exchange effects are very important. The Bloch-Brink wave function, on the other hand, is fairly well localized *outside* the core radius, and hence the effect of antisymmetrization is much less important. This external localization is reflected in the value of the spectroscopic factor $S_L \approx 0.8$, several times the SU(3) value. For such a wave function, the naive cluster picture, where one neglects exchange terms altogether, can be taken more seriously. In Fig. 3, we also show the wave function which results from the cluster model described in Sec. II. It is seen to bear a closer resemblance to the Bloch-Brink form of the cluster model than to the SU(3) model. As will be discussed presently, the simplest cluster picture also gives α widths which are in reasonable accord with experiment.

The essential reason why the Bloch-Brink wave functions yield correct α widths can be seen qualitatively from Eq. (3.5). Since γ_L involves only the

radial wave function $\mathcal{Y}_L(r)$ sampled at *one value* $r=a$, where a is usually chosen to be somewhat larger than the nuclear radius,[19,33] wave functions which are localized at large r will produce larger widths. This localization of the wave function in the surface region is one natural (although by no means unique) interpretation of the large observed α widths.

The most complete study of the problem of α widths in light nuclei is that of Arima and Yoshida.[19] These authors use a cluster wave function of the form

$$\psi_L = N_L \mathcal{A}[\mathfrak{u}_{NL}(r)\varphi_0(\xi)] \ , \tag{3.8}$$

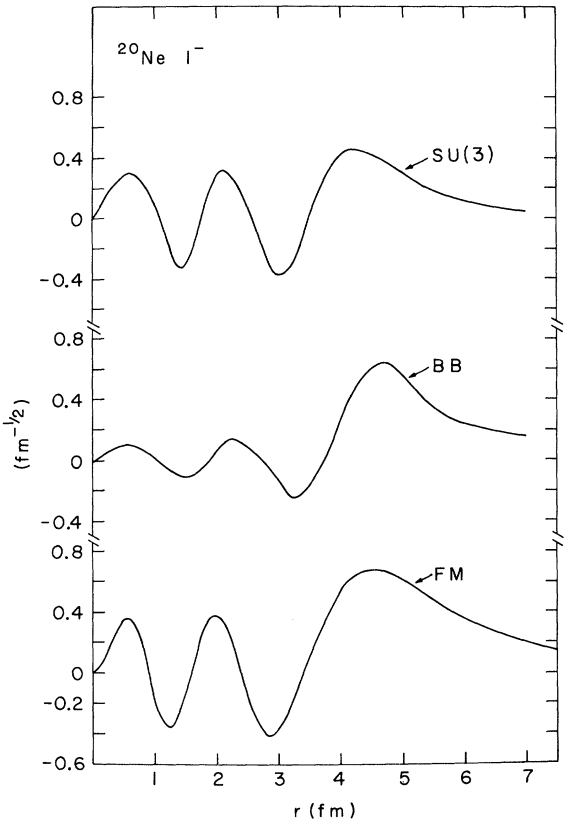

FIG. 3. Radial wave functions for the $L^\pi = 1^-$ state of the $K^\pi = 0^-$ band in ^{20}Ne. The function labeled SU(3) corresponds to the reduced width amplitude $r\mathcal{Y}_L(r)$ defined in Eq. (3.4), using the [4](90) representation of SU(3) for the composite wave function ψ_{L0} (Ref. 22). The curve labeled BB represents the function $r\mathcal{Y}_L(r)$ calculated using the Bloch-Brink antisymmetrized cluster wave function for ψ_{L0} (Refs. 9 and 22). The curve FM corresponds to the radial wave function $u_L(r)$ obtained in the unantisymmetrized cluster model, using the folding model Eq. (2.3) for the cluster potential. Note that $u_L(r)$ is normalized to unity, while $r\mathcal{Y}_L(r)$ for curves SU(3) and BB is normalized to the spectroscopic factor S_L of Eq. (3.6).

where $\varphi_0(\xi)$ is the product of internal core and cluster wave functions and $\mathfrak{u}_{NL}(r)$ is a radial wave function for the cluster, generated as a solution of the Schrödinger equation with a given single particle potential $V(r)$ of Woods-Saxon form

$$V(r) = -V_0 \Big/ \left[1+\exp\left(\frac{r-R}{a}\right)\right] \ . \tag{3.9}$$

By changing the geometry of the potential, one can clearly vary the single particle width $\Gamma_{s.p.}$ over several orders of magnitude; the procedure used in Ref. 19 is to keep the diffuseness a fixed at 0.5 fm and vary R and V_0 for *each* state in order to fit the experimental energy and α width $\Gamma_\alpha^{\exp}$ (for continuum states). Note that $\Gamma_{s.p.}$ is multiplied by the SU(3) spectroscopic factor S_L of Eq. (3.6) before comparing with $\Gamma_\alpha^{\exp}$. Arima and Yoshida[19] conclude that one must make the radius R of the potential smaller for higher spin states. This conclusion has been disputed in Ref. 18, where a single value of R and a is used for a single band, V_0 still being allowed to vary for each state.

Several disadvantages of the R-matrix formalism[19,33] should be clear from the above discussion:
(a) A purely numerical fitting procedure may lead one to draw unwarranted conclusions about the geometry of the cluster potential.
(b) The reduced width depends only on the value of $\mathcal{Y}_L(r)$ at $r=a$; it is thus quite sensitive to the choice of the channel radius a, which is not known *a priori*.
(c) Such an approach would have very little predictive power in situations where the energies and widths are not yet known experimentally.

These considerations have provided some of the motivation for a simplified cluster approach. Our choice of Eq. (2.3) for the cluster potential represents a strong theoretical prejudice as to the geometry of the potential; via Eq. (2.3), the effective radius and diffuseness of the cluster potential are uniquely related to the radii and diffusenesses of the cluster and core densities, about which we have reliable information.[12] The strength constant $\bar{f}$ of Eq. (2.3) could also in principle be estimated from the known characteristics of the free space nucleon-nucleon interaction,[13,15] but such an estimate would not be reliable for the calculation of low energy properties. We allow $\bar{f}$ to be adjustable, and find that a *single* value suffices to obtain close to the correct energy splittings within a single band. Thus we are not faced with ambiguities in the choice of potential parameters. Also, we are able to obtain the α widths of continuum states directly from the calculated α-core phase shifts; there is no need for the introduction of a channel radius and its concomitant difficulties. Finally, because of the simplicity of the model, we believe

that it possesses some predictive power, unlike a purely phenomenological approach.

We now give a summary of our results for cluster states in ^{16}O and ^{20}Ne, obtained using the folded potential of Eq. (2.3). We consider a variety of properties: (a) energy spectra; (b) α widths; (c) rms radius of composite system and mean α-core separation; (d) $B(E2)$ values.

The calculated energy spectra are shown in Figs. 4 and 5. In Fig. 4, the value of $\bar{f} = 1.425$ fm was chosen for the 0^+ band of ^{16}O, in order to position correctly the 2^+ state; the energies of the 4^+ and 6^+ states then come out very close to experiment, while the 0^+ state is a bit low. The position of the 8^+ state is not established experimentally. The $K^\pi = 0^-$ band in ^{16}O is also shown in Fig. 4. In this case, a value $\bar{f} = 1.55$ fm yields essentially the correct 3^- energy; except for the 7^- state, the energy splittings within the band are reproduced by a single value of $\bar{f}$. The corresponding spectra for the first $K^\pi = 0^+$ and 0^- bands of ^{20}Ne are shown in Fig. 5. In this case, values $\bar{f} = 1.237$ and 1.325 fm give approximately correct absolute energies of the $K^\pi = 0^+$ and 0^- bands, respectively. The energy splittings in ^{20}Ne are well reproduced by the model, except for the 8^+ state. The theoretical states lie very close to an ideal $L(L+1)$ rotational spectrum, while the experimental 8^+ state[35-37] deviates strongly from this rule. The occurrence of nearly perfect $L(L+1)$ spectra for bands with given values of $2N+L$ seems to be a general and intriguing feature of the results for folded potentials of the type described here. This striking result seems to be independent of the forms of the density functions of the interacting nuclei, provided the implied rms radii are correct. Other examples are discussed by Buck.[57]

The α widths predicted by the cluster model are shown in Table II for ^{16}O and Table III for ^{20}Ne. Since the widths are strongly dependent on energy, we have made an additional fine tuning of $\bar{f}$ for each state in order to position the levels to within a few keV of the experimental energy. The calculated widths $\Gamma_\alpha^{\text{calc}}$ can then be compared directly with experimental values. Note that only *very small* changes in $\bar{f}$ are required (a few percent) in order to fit the experimental energies. Some slight changes in the theoretical widths with respect to preliminary values published in Ref. 13 are due to the much finer tuning of the states in energy in the present work; the present values replace the more approximate results of Ref. 13.

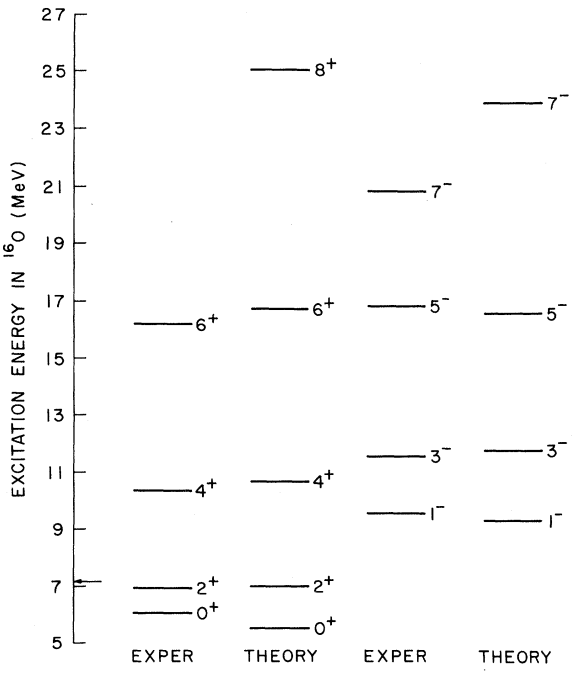

FIG. 4. $K^\pi = 0^+$ and 0^- rotational bands in ^{16}O. The experimental energies are taken from Ref. 49. The theoretical energies are obtained as the bound states and resonances of the $\alpha + ^{12}$C folded potential of Eq. (2.3). The depth parameter $\bar{f} = 1.425$ fm for the 0^+ band and $\bar{f} = 1.55$ fm for the 0^- band. The arrow indicates the position of the $\alpha + ^{12}$C threshold in ^{16}O. The widths of continuum states are tabulated in Table II.

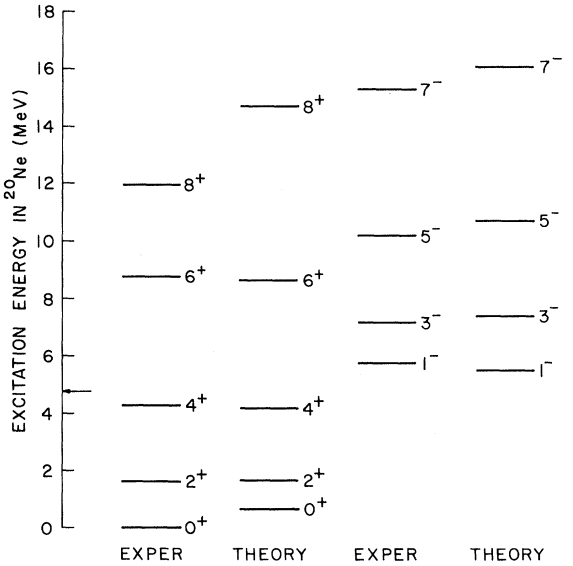

FIG. 5. Rotational bands with $K^\pi = 0^+$ and 0^- in ^{20}Ne. Experimental energies are from Ref. 24. The theoretical spectra correspond to the folded potential of Eq. (2.3) with $\bar{f} = 1.237$ fm for the ground state band and $\bar{f} = 1.325$ fm for the negative parity band. The arrow indicates the $\alpha + ^{16}$O threshold in ^{20}Ne; the widths of α-cluster states above threshold are displayed in Table III.

TABLE II. Calculated and experimental α widths for ^{16}O.

J^π	Γ_α^{exp} (keV)	Γ_α^{calc} (keV)	$\bar{f}$ (fm)
	$K^\pi = 0^+$ band		
4^+	27	17.5	1.436
6^+	125	238	1.432
8^+	···	385	1.425
	$K^\pi = 0^-$ band		
1^-	510	675	1.536
3^-	1200	1750	1.5575
5^-	700	≈2000	1.539
7^-	750	776	1.668

Within a factor of 2 or so, the theoretical and experimental widths are in essential agreement. The theoretical widths Γ_α^{calc} are obtained directly from the calculated phase shifts as the energy interval over which the phase shift changes from $\frac{1}{4}\pi$ to $3\pi/4$; this prescription is valid for narrow resonances or if the width function $\Gamma_\alpha(E)$ is not rapidly energy dependent. As an example, we plot in Fig. 6 the function $\sin 2\delta_L$ as a function of energy for the $L=1$, 3, and 5 single particle resonances in the $\alpha + {}^{16}$O scattering system, using the folded potential of Eq. (2.3). Figure 6 shows that the calculated phase shifts δ_L are very close to 0 or π except in the immediate vicinity of the resonance. That is, in most cases these resonances can be very well fitted by a pure Breit-Wigner form

$$\sin 2\delta_L(E) = \frac{\Gamma_L(E)(E_R - E)}{(E_R - E)^2 + [\Gamma_L(E)/2]^2} \tag{3.10}$$

without any background term. Only the $L=3$ resonance requires a small background contribution. In Eq. (3.10), E_R is the center of mass (c.m.) resonance energy, E is the c.m. energy, and $\Gamma_L(E)$ is the width function. In obtaining the fits to the calculated points in Fig. 6, we have used the form

$$\Gamma_L(E) = \Gamma_L(E_R)(E/E_R)^{L+1/2} \tag{3.11}$$

which includes the pentrability factor P_L of Eq. (3.2) in an approximate way. The energy dependence of the width $\Gamma_L(E)$ enables us to reproduce the asymmetry of the resonance shape without introducing a background term, except for $L=3$. As expected, $\Gamma_L(E_R)$ is nearly identical to the width obtained by taking the energy interval over which $\sin 2\delta_L$ changes from $+1$ to -1 (δ_L from $\frac{1}{4}\pi$ to $3\pi/4$).

If one naively calculates a spectroscopic factor as the ratio of the experimental width Γ_α^{exp} to the single particle width $\Gamma_\alpha^{calc} \approx \Gamma_L(E_R)$, one might be led to conclude that these states possess a greater degree of cluster structure than suggested by the SU(3) model. However, the calculated widths would be very sensitive to the addition of an imaginary part to the depth parameter $\bar{f}$, so such a conclusion is premature. Note than we do not expect the imaginary part to be very large, since there are no other open channels in ^{20}Ne beside $\alpha + {}^{16}$O in the energy range up to 12.85 MeV excitation energy, where the ^{19}F $+p$ channel opens up. All of the states we consider, except the 7^- and 9^- members of the $K^\pi = 0^-$ band, lie below the ^{19}F $+p$ threshold.

The calculated widths Γ_α^{calc} are also in excellent agreement with the values Γ_α^{BB} listed in Table III, calculated[22] using the Bloch-Brink form of the cluster model. The values without parentheses are obtained using the separation energy method for attaching a proper exponential tail to an oscillator wave function, while the values in parentheses are obtained via a Green's function method.[22] This agreement with the Bloch-Brink model

TABLE III. Calculated and experimental α widths for ^{20}Ne.

J^π	Γ_α^{exp} (keV)	Γ_α^{calc} (keV)	$\bar{f}$ (fm)	$\Gamma_\alpha^{SU(3)}$ (keV)	Γ_α^{BB} (keV)
		$K^\pi = 0^+$ band			
6^+	0.11	0.21	1.232		
8^+	0.035	0.108	1.291		
		$K^\pi = 0^-$ band			
1^-	> 0.013	0.021	1.313	0.0024 (0.0024)	0.0135 (0.0108)
3^-	8	6.7	1.3274	0.8 (1.16)	5.0 (5.6)
5^-	141	81.0	1.339	9.3 (18.6)	74.5 (70.5)
7^-	280	183.0	1.345	14.2 (39.0)	198.0 (184.0)

is not surprising, since the spectroscopic factor S_L of Eq. (3.6) is about 0.8 for this model. We are thus close to the limiting case where exchange effects are small and the cluster is relatively well localized outside the core; these are precisely the conditions under which our simple cluster model retains some validity. The SU(3) width predictions[22] are also shown in Table III for the $K^\pi = 0^-$ band of ^{20}Ne; as remarked earlier the SU(3) widths are more than an order of magnitude too small, which could indicate insufficient localization of the cluster in the surface.

The fact that the folded potential gives approximately the correct α widths can be understood qualitatively by a consideration of Fig. 7, where

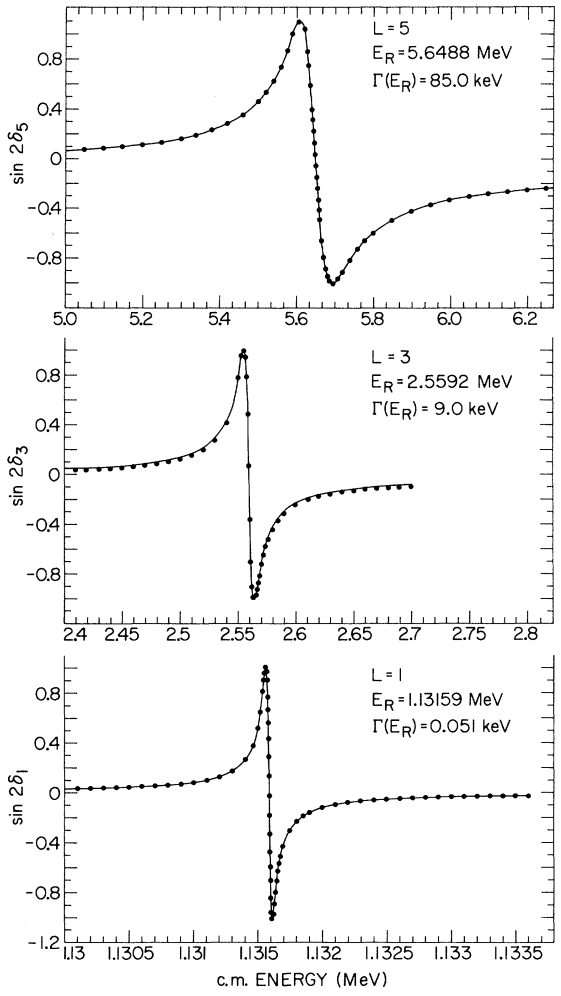

FIG. 6. Single particle resonances in the $\alpha + ^{16}$O scattering system using the folded potential of Eq. (2.3). The states shown correspond to the 1^-, 3^-, and 5^- members of the $K^\pi = 0^-$ band in ^{20}Ne. We have used depth parameters $\bar{f} = 1.313$, 1.3274, and 1.339 fm in Eq. (2.3) for the 1^-, 3^-, and 5^- states, respectively. We plot $\sin 2\delta_L$ vs the center of mass energy for each state, where δ_L is the phase shift and the energy is measured with respect to the $\alpha + ^{16}$O threshold in ^{20}Ne. The solid points represent the results of calculating the potential scattering phase shifts δ_L directly using program ABACUS (Ref. 48). The solid curves represent an empirical fit to the calculated phase shifts using the single pole approximation of Eq. (3.10). The resonance energy E_R and width at resonance $\Gamma(E_R)$ corresponding to each solid curve are shown on the figure. Slight differences between these parameters and the more precise values given in Table III and Fig. 5 are due to using a smaller cutoff radius (9 fm) for the nuclear potential.

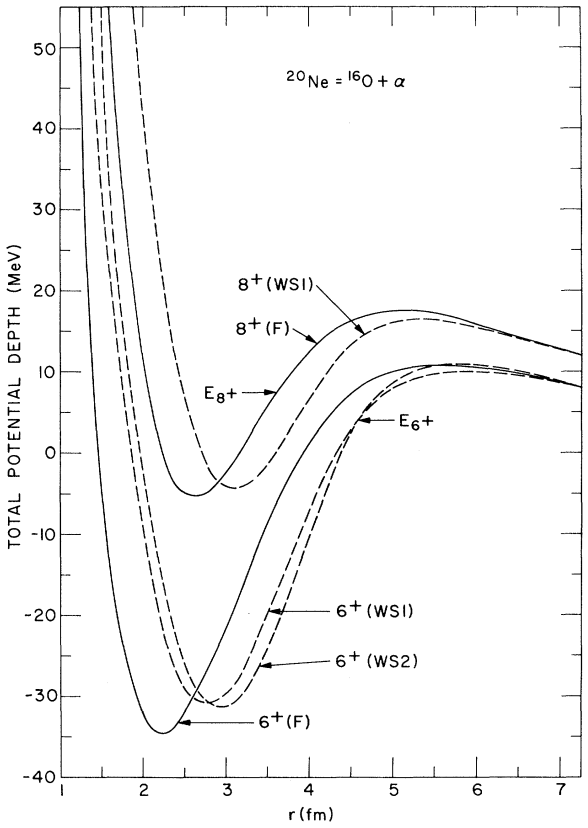

FIG. 7. Total potential depth, including nuclear, Coulomb, and centrifugal contributions, for the 6^+ and 8^+ states of the ^{20}Ne ground state band. The solid curves labeled 6^+(F) and 8^+(F) correspond to the folded potential of Eq. (2.3) for the $\alpha + ^{16}$O case. The dashed curves labeled WS1 correspond to the Woods-Saxon nuclear potential of Mosley and Fortune (Ref. 18), while the 6^+ curve labeled WS2 is from Arima and Yoshida (Ref. 19). The potential WS2 is of the form of Eq. (3.9), with $R = 3.78$ fm, $V_0 = 83.46$ MeV, and $a = 0.5$ fm. In all cases, the Coulomb potential is taken to be that of a uniform sphere of radius 3.53 fm. The depth of the nuclear potential has been adjusted to fit the experimental 6^+ and 8^+ energies in each case; these energies are indicated by the symbols E_{6+} and E_{8+} in the figure. For the folded potential, this required depth parameters $\bar{f} = 1.232$ and 1.291 fm for the 6^+ and 8^+ states, respectively.

we display the *total* potential depth (nuclear + Coulomb + centrifugal) for the 6^+ and 8^+ members of the ground state band in ^{20}Ne. The folded potential (solid line) is seen to give a somewhat higher and wider barrier than Woods-Saxon potentials[18,19] which have also been adjusted to give the experimental binding energies. This is mainly due to the large effective diffuseness of the folded potential, as displayed in Fig. 2. As a consequence of the larger barrier, the penetrabilities for the folded potential are smaller than those for the Woods-Saxon potentials[18,19] and hence, the corresponding single particle widths are also smaller. Note, however, that the Woods-Saxon potentials[18,19] also give about the correct experimental α widths $\Gamma_\alpha^{\exp}$ for the 6^+ and 8^+ states, since the single particle width is multiplied by the SU(3) spectroscopic factor $S_L = 0.23$ of Eq. (3.6) before comparing with experiment. For the folded potential, we get a considerably smaller single particle width, but since $S_L = 1$ for the simple cluster model (and also close to 1 for antisymmetrized cluster models[9,22]), we identify the single particle width directly with the experimental value.

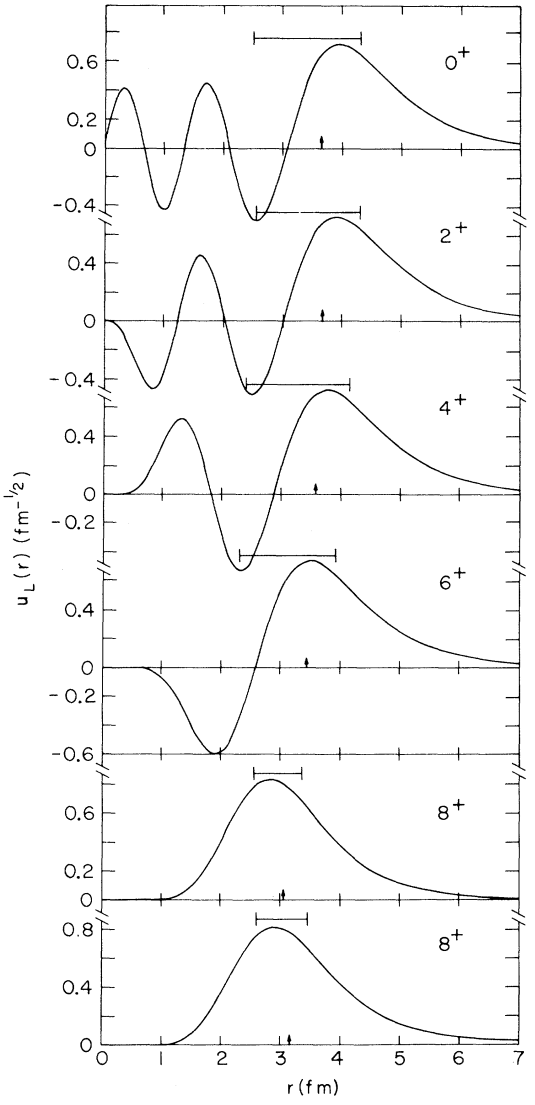

FIG. 8. Radial wave function $u_L(r)$ for the $K^\pi = 0^+$ ground state band of ^{20}Ne in the cluster model. For each curve, the arrow corresponds to the rms α-^{16}O separation ρ of Eq. (3.12). The bracket above each curve gives the mid 50% of the probability distribution for the α cluster; these brackets indicate the degree of localization of the α cluster. The first five curves correspond to α clusters having close to the experimental binding energies; we have $\bar{f} = 1.2523$, 1.237, 1.237, 1.2318, and 1.291 fm for the 0^+, 2^+, 4^+, 6^+, and 8^+, respectively. The final curve for the 8^+ state corresponds to the spectrum shown in Fig. 5, for which $\bar{f} = 1.237$ fm. The continuum wave functions for the 6^+ and 8^+ states are normalized to unity in a box of radius 7.5 fm.

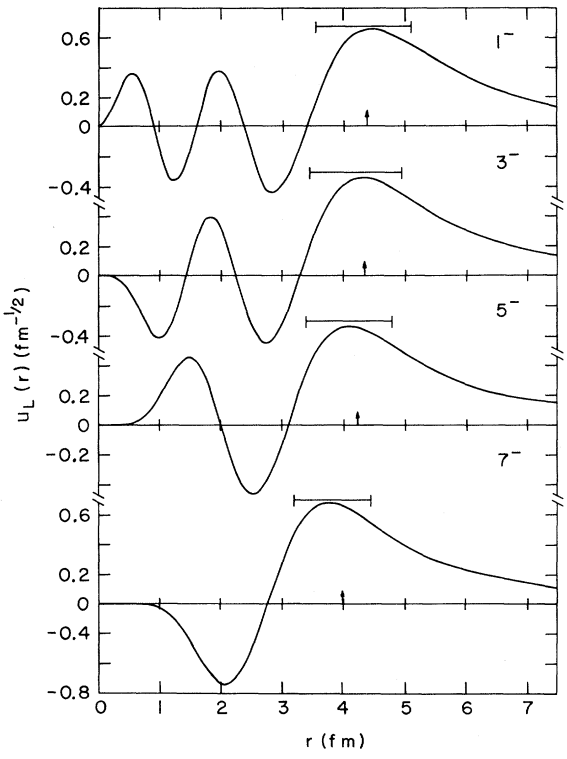

FIG. 9. Cluster model wave functions $u_L(r)$ for the $K^\pi = 0^-$ band of ^{20}Ne (9^- state omitted). For each curve, the arrow corresponds to the rms α-nucleus separation ρ of Eq. (3.10) and the bracket gives the mid 50% of the α-cluster probability. Each wave function corresponds to a state at the observed energy: values $\bar{f} = 1.313$, 1.3274, 1.339, and 1.345 fm have been used to correctly position the 1^-, 3^-, 5^-, and 7^- states, respectively. All wave functions are normalized in a box of radius 7.5 fm.

TABLE IV. α-core separation ρ and rms radii for the ground state band in ^{20}Ne.

J^π	ρ (fm)	$\rho^{(1)}$ (fm)	$\rho^{(2)}$ (fm)	$\rho^{(3)}$ (fm)	$\langle r^2\rangle_{20}^{1/2}$ (fm)
0^+	3.67	3.82	3.75	3.86	2.96
2^+	3.68	3.85	3.78	3.84	2.97
4^+	3.58	3.81	3.76	3.76	2.95
6^+	3.44	3.78	3.76	3.67	2.92
8^+	3.06	3.48	3.56	3.54	2.85

TABLE V. Electromagnetic transition rates for the ground state band of ^{20}Ne.

Transition	$B(E2)_{\text{exp}}$ [a]	$B(E2)$	$B(E2)_{\text{SM}}$	$B(E2)_{\text{RM}}$
$2^+ \rightarrow 0^+$	57.3	57.3	52.6	57.6
$4^+ \rightarrow 2^+$	71.0	73.8	64.5	82.4
$6^+ \rightarrow 4^+$	66.0	62.7	53.4	90.8
$8^+ \rightarrow 6^+$	24.0	28.9	32.8	95.6

[a] All $B(E2)$ values in units of $e^2\,\text{fm}^4$.

In Figs. 8 and 9, we show the radial wave functions $u_{NL}(r)$ for the $K^\pi = 0^+$ and 0^- bands of ^{20}Ne, obtained using the folded potential of Eq. (2.3). The rms separation ρ of the α cluster from the ^{16}O core, defined by

$$\rho^2 = \int_0^\infty r^2 u_{NL}^2 dr \tag{3.12}$$

is indicated by an arrow for each state. The radial wave function $u_{NL}(r)$ is normalized so that $\int u_{NL}^2(r)dr = 1$. A bracket is also given such that the middle 50% probability region for the cluster-core separation is localized within the bracket, 25% above the indicated region and 25% below. As seen from Figs. 8 and 9, most of the α-cluster probability is located well outside the calculated rms radius of the ^{20}Ne composite system, shown in Table IV. These wave functions are very similar to those of the Bloch-Brink cluster model[9,22] and hence, rather distinct from SU(3) wave functions, which have a much greater overlap with the nuclear interior. In view of these properties, it seems that we are justified *a posteriori* in neglecting exchange effects for this case.

The values of ρ for the various states of the ^{20}Ne ground state band are shown in Table IV. The rms radius $\langle r^2\rangle_{20}^{1/2}$ of the ^{20}Ne composite system computed from

$$\langle r^2\rangle_{20} = \tfrac{4}{5}\langle r^2\rangle_{16} + \tfrac{1}{5}\langle r^2\rangle_\alpha + \tfrac{4}{25}\rho^2 \tag{3.13}$$

is also given for each of the states. To calculate $\langle r^2\rangle_{20}$, we used $\langle r^2\rangle_{16} = (2.75)^2$ fm^2 and $\langle r^2\rangle_\alpha = (1.71)^2$ fm^2, which correspond to the radii of the densities used to generate the folded potential of Eq. (2.3). In Table IV we also show the results of a variety of other calculations of ρ: $\rho^{(1)}$ and $\rho^{(2)}$ are obtained from Refs. 18 and 19, respectively, using Woods-Saxon potentials to generate the α-cluster wave functions; $\rho^{(3)}$ is obtained from the Hartree-Fock calculations of Ref. 28. Several features of Table IV are noteworthy: (a) Even though the α cluster is localized at the surface, the folding model yields essentially the correct value for the rms radius of ^{20}Ne; the theoretical value of 2.96 fm agrees well with the empirical value 2.9 fm given in Ref. 38. (b) All the theoretical models in Table IV predict an anticentrifugal stretching effect, i.e., the *higher* spin states corresponds to a *lower* value of ρ and hence, a smaller rms radius. In the folding model, as in Ref. 18, this effect does *not* require a change in radius of the potential itself; the folded potential has a fixed geometry for all the states. The anticentrifugal stretching effect arises from a competition between the increasing L value, which tends to increase ρ and a decreasing number of nodes, which favors a smaller ρ. Whether one gets centrifugal stretching or anticentrifugal stretching thus depends on the details of the potential. If we have an oscillator potential, for instance, ρ would be the same for each state within a band (fixed value of $2N+L$). The effective diffuseness of the potential is clearly of relevance. For a very small diffuseness, we would expect to get centrifugal stretching (i.e., limit of a square well); for a large effective diffuseness, as is the case for the folded potential, we expect anticentrifugal stretching. Relative to the Woods-Saxon and the Hartree-Fock models, the folded potential gives the largest amount of anticentrifugal stretching.

As a final test of our model, we calculate the electromagnetic transition rates between levels of a rotational band. We treat these transitions in a pure single particle model, for which the $B(E2)$ value for ^{20}Ne is given by

$$B(E2) = \frac{16}{5\pi} e_{\text{eff}}^2 (u_{N,L+2}|r^2|u_{N,L})^2 (L+2, 020|L0)^2 \tag{3.14}$$

for a transition $L+2 \rightarrow L$, where e_{eff} is the effective charge given by $e_n + e_p$, where $e_n = \epsilon e$ and $e_p = (1+\epsilon)e$ are neutron and proton effective charges. The resulting values are tabulated in Table V. We also give the experimental values $B(E2)_{\text{exp}}$ [35,36] and the results of other theoretical calculations in the shell model $[B(E2)_{\text{SM}}]$ and the simple rotational model $[B(E2)_{\text{RM}}]$.[16] Several remarks are in order: With only a small adjustment of the effective charge $e_{\text{eff}} = 1.245e$ or $\epsilon = 0.123$, the folding model yields values $B(E2)$ rather close to the results $B(E2)_{\text{SM}}$ of the complete shell-model calculation[24] which used $e_{\text{eff}} = 1.583e$. In particular, the cluster

TABLE VI. Predicted transition rates for the first $K^\pi = 0^-$ band in ^{20}Ne and the first $K^\pi = 0^+$ and 0^- bands in ^{16}O.

Transition	$B(E2)$ (e^2 fm^4)	$B(E2)$	$B(E2)_{exp}$ [a]
	^{20}Ne		
$3^- \to 1^-$	100.3 [b]	76.9,[c] 143.0 [c]	
$5^- \to 3^-$	103.5		
$7^- \to 5^-$	84.0		
	^{16}O		
$2^+ \to 0^+$	66.8 [d]	30 [e]	67
$4^+ \to 2^+$	89.1	32	116 ± 15
$6^+ \to 4^+$	91.1	21	
$8^+ \to 6^+$	52.9	22	
$3^- \to 1^-$	152.6 [b]	15 [e]	
$5^- \to 3^-$	97.5	23	
$7^- \to 5^-$	76.77	17	

[a] References 53 and 59.
[b] $e_{eff} = e$.
[c] See Ref. 16. $e_{eff} = 2.166e$.
[d] $e_{eff} = 1.246e$.
[e] See Ref. 59. $e_{eff} = 2e$.

model produces the *trend* of $B(E2)$ values, i.e., the $4^+ \to 2^+$ transition is strongest and the $8^+ \to 6^+$ weakest. Note that the rotational model $B(E2)_{RM}$ predicts that the $8^+ \to 6^+$ transition is the strongest, in disagreement with the data. Thus although the cluster model gives close to an $L(L+1)$ rotational energy spectrum, the $B(E2)$ values are far from the rotational limit.

The predicted $B(E2)$ values for the $K^\pi = 0^-$ band in ^{20}Ne are shown in Table VI, as well as the values for the first $K^\pi = 0^+$ and 0^- bands in ^{16}O. For the negative parity states in Table VI, the bare charge was used in the folding calculations, due to the absence of experimental data. For ^{20}Ne, we compare with some results of Arima *et al.*[16] for the $3^- \to 1^-$ transition, which use two different residual interactions in the shell-model calculation and $e_{eff} = 2.166e$. For the positive parity states in ^{16}O, we have used the *same* effective charge $e_{eff} = 1.246e$ ($\epsilon = 0.123$) as was used in Table V to fit the $2^+ \to 0^+$ $B(E2)$ value in ^{20}Ne; the resultant agreement with the experimental values[53,59] in ^{16}O is remarkable. This agreement is particularly noteworthy since only a *small* renormalization of the effective charge is required. On the other hand, the shell-model $B(E2)$ values[59] for the first $K^\pi = 0^+$ band in ^{16}O are consistently too small by more than a factor of 2, even with a much larger effective charge. This difference is traceable to the greater degree of *surface localization* for the cluster wave functions as compared to shell-model wave functions. Such localization enhances both the $B(E2)$ values and the α widths with respect to shell-model or SU(3) predictions, and brings the results into agreement with experiment. Note that the shell-model wave functions[59] for the first $K^\pi = 0^+$ band in ^{16}O are predominantly of four particle-four hole character, consistent with our cluster model assignment of $2N + L = 8$, but the shell model in a restricted basis of states does not seem to develop enough correlations in the nuclear surface.

For the transitions between the members of the $K^\pi = 0^-$ band in ^{16}O (see Table VI), the cluster model predicts $B(E2)$ values which differ from shell-model predictions[59] by more than an order of magnitude if the same effective charge is employed. However, the shell-model 1^-, 3^-, 5^-, and 7^- states in ^{16}O are mostly three particle-three hole in nature,[59] and hence, would correspond to the $2N + L = 7$ cluster band. We have instead identified the 1^-, 3^-, 5^-, and 7^- states in ^{16}O with the $2N + L = 9$ cluster band. Here we follow an argument of Arima and Yoshida,[19] who point out that in a weak coupling picture, the first $K^\pi = 0^-$ band in ^{16}O should be analogous to the first $K^\pi = 0^-$ band in ^{20}Ne, i.e., $2N + L = 9$. Of course, since the shell-model calculation[59] does not include the $2p$-$1f$ shell, no states corresponding to $2N + L = 9$ can be obtained. Experimental measurements of the electromagnetic transition rates in the $K^\pi = 0^-$ bands of ^{16}O and ^{20}Ne would be extremely valuable in determining the nature of these states. Since all the negative parity states in Table VI, as well as the 6^+ and 8^+ members of the ground state band in ^{20}Ne, are above the α-emission threshold, experimental measurements are very difficult; only for the $8^+ \to 6^+$ does a measurement exist.[36] In the cluster calculation, we have used a box normalization for the continuum states. The calculated transition rates depend only rather weakly on the cutoff R, if R is chosen within reasonable limits. For the 6^+ and 8^+ states in ^{20}Ne, we use $R = 7.5$ fm. For the $K^\pi = 0^-$ band in ^{20}Ne and the two bands in ^{16}O, we use $R = 8$ fm. The 9^- state lies high in the continuum, and has a large width, so we have omitted it from our study.

Let us now briefly summarize the results of our study of α-cluster states in ^{16}O and ^{20}Ne:

(a) The folded potential Eq. (2.3) produces a spectrum with essentially the correct level order and energy spacing, utilizing a single value of the depth parameter $\bar{f}$ per band.

(b) The calculated α widths are in reasonable agreement with experiment.

(c) The α-cluster wave functions are fairly well localized outside the ^{16}O core; in spite of this, the ^{20}Ne composite system has the correct rms radius.

(d) The absolute values and trends of the electromagnetic transition rates for the ground state

TABLE VII. Possible high-spin states in ^{15}N seen in three particle transfer reactions.

E_{exc} (MeV)	E_t (MeV)	J^π
5.27	−9.58	$\frac{5}{2}^+$
7.56	−7.29	$\frac{7}{2}^+$
9.87	−4.98	$\frac{7}{2}^{(-)}$
10.78	−4.07	$(\frac{9}{2}^+)$
13.15	−1.70	$\frac{11}{2}^-$
15.72	+0.87	$(\frac{13}{2}^+)$

band of ^{20}Ne and the band based on the 6.06 MeV 0^+ state in ^{16}O are in good agreement with experiment, using only a small renormalization of the effective charge.

For the well-known case of ^{20}Ne, there seems to be no glaring discrepancy between the predictions of the simple cluster model and experimental data. We are hence encouraged to try out the model in situations where the energies and spins of possible cluster states are not established. As an example of the use of the folding model as a predictive tool, we consider such a case in the next section.

IV. THREE PARTICLE CLUSTER STATES

Recently, a variety of three particle transfer reactions have been studied experimentally.[1,2,39-42] These reactions exhibit strong selectivity, in addition to the selectivity which arises from L transfer and Q-value dependence. The data seem to be consistent with a direct three nucleon transfer mechanism. Under conditions of large momentum mismatch, the kinematical selection rules of Brink[7] suggest the preferential population of high-spin states.[2,8] For example, in reactions such as (^{6}Li, ^{3}He), (^{7}Li, α), and (^{10}B, ^{7}Be) on a ^{12}C target[1,39-42] certain states in ^{15}N are strongly populated in all cases. Such states are candidates for a triton cluster interpretation; the analog states in the ^{15}O system would correspond to a ^{3}He cluster plus a ^{12}C core. The states in question are listed in Table VII. The energies E_{exc} and E_t are, respectively, the excitation energy in ^{15}N and the energy above the $t+^{12}$C threshold. The spins of the $\frac{9}{2}^+$ and $\frac{13}{2}^+$ states are based on the Brink selection rules; the $\frac{11}{2}^-$ state is also seen in two particle transfer.[7,43,44] The suggested $\frac{9}{2}^+$ state coincides very closely in energy with a well established $\frac{3}{2}^-$ state seen in the ^{13}C(^{3}He, $p\gamma$)^{15}N reaction.[45] We would not expect to observe a high-spin state such as a $\frac{9}{2}^+$ in the latter reaction, however.

TABLE VIII. Cluster model states for ^{15}N and ^{15}O.

N	L	J^π
	$2N+L=3$ band	
1	1	$\frac{1}{2}^-$ $(\frac{3}{2}^-)$
0	3	$(\frac{5}{2}^-)$ $(\frac{7}{2}^-)$
	$2N+L=4$ band	
2	0	$\frac{1}{2}^+$
1	2	$\frac{3}{2}^+$ $\frac{5}{2}^+$
0	4	$\frac{7}{2}^+$ $(\frac{9}{2}^+)$
	$2N+L=5$ band	
2	1	$\frac{1}{2}^-$ $\frac{3}{2}^-$
1	3	$\frac{5}{2}^-$ $\frac{7}{2}^-$
0	5	$\frac{9}{2}^-$ $\frac{11}{2}^-$
	$2N+L=6$ band	
3	0	$\frac{1}{2}^+$
2	2	$\frac{3}{2}^+$ $\frac{5}{2}^+$
1	4	$\frac{7}{2}^+$ $\frac{9}{2}^+$
0	6	$\frac{11}{2}^+$ $\frac{13}{2}^+$

In the context of the simple cluster model, we interpret the states in Table VII in terms of a triton cluster in a certain orbit characterized by principal quantum number N and orbital quantum number L with respect to an inert ^{12}C core. The four bands we will consider are listed in Table VIII. These bands correspond to the various ways of distributing three particles in the $1p$ or $2s$-$1d$ shells, i.e., $2N+L=3$ corresponds to putting all three particles in the $1p$ shell; $2N+L=4$ corresponds to two $1p$ particles and one $1s$-$2d$ particle, etc. In terms of the usual shell model based on an ^{16}O core, $2N+L=3, 4, 5, 6$ bands correspond to one hole (h), zero particle (p), 2h-1p, 3h-2p, and 4h-3p configurations, respectively. The states enclosed in parentheses in Table VIII are explicitly excluded by the Pauli principle. For the $2N+L=3$ band, only the $\frac{1}{2}^-$ state survives, which would be identified with the ^{15}N ground state. Of course there is no reason to expect that the cluster picture is correct for such low-lying low-spin states. In particular, the cluster representation for the ^{15}N ground state probably has very little overlap with the true ground state. For such deeply bound states, the effect of the Pauli principle will be very important. Hence we concentrate most of our attention on the high-spin states in the $2N+L=5$ and 6 bands; it is some of these states that we will try to identify with the high-spin states in Table VII.

A few words of caution are in order before we proceed. It should be noted that the *same* states in the residual nucleus are not populated with the same relative intensities in different reactions in which a given cluster is transferred, for example, (^{7}Li, α), (^{10}B, ^{7}Be), (^{19}F, ^{16}O), and (α, p). This is to be expected, since the detailed *dynamics* of the transfer is different in each case; thus one should supplement the simple considerations given here by the appropriate distorted wave Born approximation calculation of the transfer cross sections, assuming that the three particles are transferred as a cluster.[41] Such detailed calculations of three and four particle transfer will be presented in a subsequent article.[46] We note that the overall spectroscopic factor for a transfer reaction $A+B \rightarrow (A-m)+(B+m)$ does not factorize in general into a term depending only on A and $A-m$ and another term which depends only on B and $B+m$.[47] Hence, the relative population of states in m particle transfer must be determined by a detailed dynamical calculation; it cannot be reliably predicted by kinematical conditions alone. In a reaction calculation, one can also ask in what state of orbital symmetry the transferred particles find themselves. In the (α, p), (^{7}Li, α), and (^{19}F, ^{16}O) reactions, the three transferred particles have the orbital symmetry [3], i.e., the same as the triton. However, for the (^{10}B, ^{7}Be) reaction, the three particles can be transferred in a [21] orbital symmetry as well as the fully symmetric [3] configuration. Hence the interpretation of such results in terms of a simple "triton" transfer must be viewed with caution.

We have previously noted the considerable overlap between the shell model and the antisymmetrized cluster model. It is perhaps also worthwhile to note the nonuniqueness of a cluster description; for ^{15}N, one could propose $t+^{12}$C, $\alpha+^{11}$B, $d+^{13}$C cluster representations, among others. These different models differ somewhat in the spins they predict and the number of states. In cases where the high-spin states are not well established experimentally, it is difficult to choose between models on this basis. Also, some of the

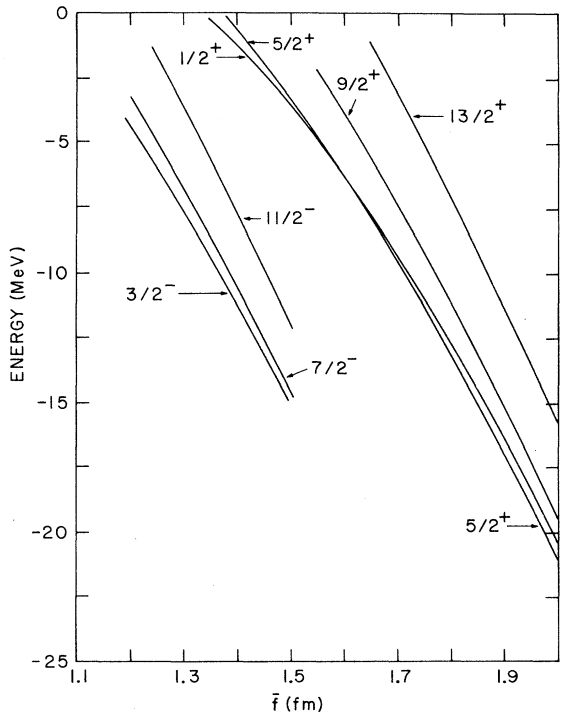

FIG. 10. Dependence of the ^{3}H+^{12}C cluster state energies in ^{15}N on the depth parameter $\bar{f}$ of the folded potential of Eq. (2.3). The energy is given with respect to the ^{3}H+^{12}C threshold at 14.85 MeV in ^{15}N. The orbits shown are the $J=L+\frac{1}{2}$ members of the $2N+L=5$ band ($\frac{3}{2}^-$, $\frac{7}{2}^-$, $\frac{11}{2}^-$) and the $2N+L=6$ band ($\frac{1}{2}^+$, $\frac{5}{2}^+$, $\frac{9}{2}^+$, $\frac{13}{2}^+$). A spin-orbit strength $V_{so}=0.05$ was used.

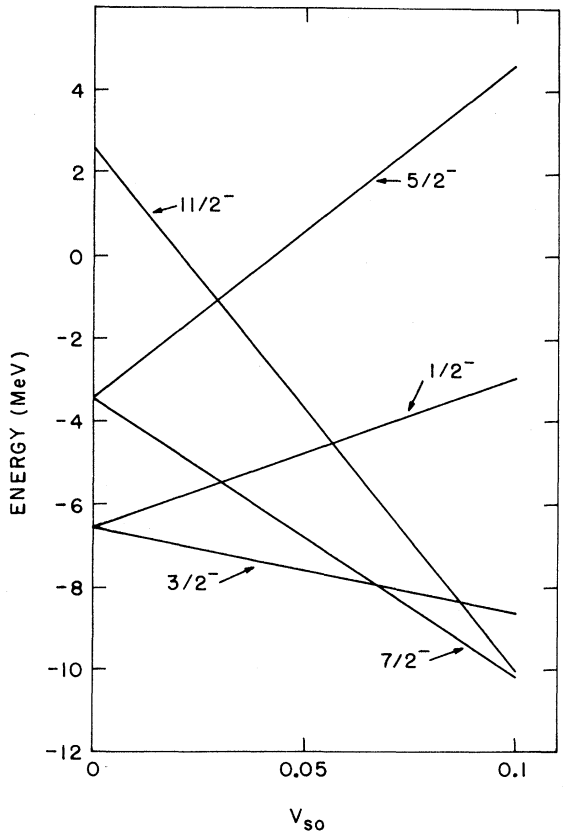

FIG. 11. Dependence of the ^{3}H+^{12}C cluster state energies in ^{15}N on the strength V_{so} of the spin-orbit potential, for a fixed value $\bar{f}=1.3$ fm of the depth parameter. The energy is given with respect to the ^{3}H+^{12}C threshold in ^{15}N. The states shown are members of the $2N+L=5$ cluster band.

same high-spin states are strongly excited in *different* cluster transfer reactions, for example, ^{11}B(^{7}Li, t)^{15}N and ^{12}C(^{7}Li, α)^{15}N *both* strongly excite[42] the 10.8, 13.2, and 15.7 MeV states of Table VII. Such results indicate a high degree of overlap between alternate cluster descriptions. Note also that cluster models of the type discussed here always predict a maximum spin for a band with a given value of $2N+L$. This maximum spin is $j_{max}=2N+L$ for α clusters and $j_{max}=2N+L+\frac{1}{2}$ for ^{3}He or ^{3}H clusters. If a state of higher spin than j_{max} is seen experimentally, the simple cluster model clearly cannot be valid for this state; an example would be a 10^+ member of the ground state rotational band of ^{20}Ne. Both the shell model and the cluster model will accommodate spins higher than the maximum, provided core excitations are allowed. However, in the various rotational bands of ^{12}C, ^{16}O, and ^{20}Ne, no state has yet been observed which has a spin higher than the cutoff implied by the α-cluster model built on an unexcited ^{16}O core. If we take this prediction literally for t or ^{3}He clusters in ^{15}N, a maximum spin of $\frac{13}{2}^+$ is indicated (unless we start to drop particles in the $1f$-$2p$ shell). This is the same as the maximum spin attainable in the shell model from the configuration $[(d_{5/2})^2_5+\otimes\, d_{3/2}]_{13/2+}$ if the ^{12}C remains inert.

Now let us consider the results of our numerical calculations for the states of ^{15}N, viewed as $t+^{12}$C cluster states, with special emphasis on the $2N+L=5$ and 6 bands of Table VIII. Bound state energies corresponding to the folded potential of Eqs. (2.2)–(2.4) have been computed using a version of the code ABACUS.[48] Trajectories of the various bound states as a function of the well depth parameter $\bar{f}$ are displayed in Fig. 10, for a value $V_{so}=0.05$ of the spin-orbit strength. In Fig. 11, we show the dependence of the $2N+L=5$ bound state energies on V_{so} for a fixed central depth $\bar{f}=1.3$ fm.

For the $2N+L=5$ band, we have adjusted $\bar{f}$ and V_{so} to obtain the correct absolute energy and energy splitting for the $\frac{11}{2}^-$ and $\frac{7}{2}^-$ states in Table VII. The resulting cluster spectrum is shown as the second column in Fig. 12. As a bonus, the $\frac{3}{2}^-$ and $\frac{1}{2}^-$ cluster states show up in a region where such states are seen experimentally. Kinematically, such low-spin states would not show up clearly in high energy heavy ion transfer.[7] However, in the lower energy (30 MeV) (^{6}Li, ^{3}He) data of Bassani *et al.*[39] and Chuev *et al.*[40] there is a moderate peak at 9.2 MeV in ^{15}N which could be identified with the $\frac{3}{2}^-$ cluster state (and with the $\frac{3}{2}^-$ state at −5.7 MeV in column 1 of Fig. 10). The analog in ^{15}O is probably the 8.93 MeV state.[49] Also in Refs. 39 and 40 there are small peaks seen at 11.4 MeV in ^{15}N and 11.2 MeV in ^{15}O which could possibly correspond to the $\frac{1}{2}^-$ cluster states.

In columns 3 and 4 of Fig. 12, we show typical spectra obtained without a cluster spin-orbit potential. In column 3, $\bar{f}$ is adjusted to give $\frac{1}{2}^-$ and $\frac{3}{2}^-$ states in the energy range of observed states. In this case, the $\frac{9}{2}^-$ and $\frac{11}{2}^-$ states lie much too high in energy, about 7–8 MeV above the observed energies. In column 4, $\bar{f}$ is chosen to position the $\frac{11}{2}^-$ state at the experimental energy; in this case the $\frac{1}{2}^-$ and $\frac{3}{2}^-$ states lie within a few MeV of the ground state. In this region, there are no candidates for identification with cluster states. In either case, the cluster model without spin-orbit coupling yields a spectrum which is too spread out in energy, and hence, one runs into obvious

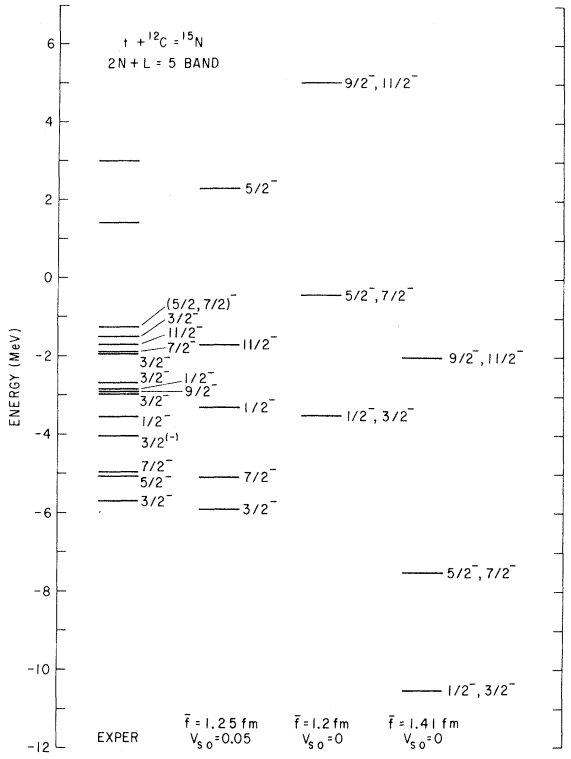

FIG. 12. Some theoretical spectra for ^{3}H+^{12}C cluster states in ^{15}N, corresponding to the $2N+L=5$ band. Experimentally observed negative parity states in the energy region of interest are also shown (Ref. 49) in the column labeled Exper. The upper two states correspond to states of unknown spin and parity seen relatively strongly in the ^{12}C(^{10}B, ^{7}Be)^{15}N reaction (Ref. 1). The second column corresponds to a choice of $\bar{f}$ and V_{so} which reproduces the experimental $\frac{11}{2}^-$ energy and also the $\frac{7}{2}^- - \frac{11}{2}^-$ energy difference. For this choice, the $\frac{9}{2}^-$ state lies at 12.7 MeV in the continuum. The last two columns are the theoretical spectra obtained if one neglects the spin-orbit potential.

inconsistencies with the experimental data. Of course, as discussed in detail for the ^{20}Ne case, the energy splittings depend strongly on the geometry of the potential. However, in the present case, we regard the geometry as fixed by our knowledge of nuclear densities. Hence, the level compression which we need in order to make a meaningful comparison with experiment is most naturally provided by the spin-orbit potential. The value $V_{so} = 0.05$ which we obtain here is comparable to what one might naively expect on the basis of the proton-nucleus spin-orbit potential, scaled down by the number of particles in the cluster. Thus, we feel that the experimental spectra observed in three nucleon reactions[1,2,39-42], *if* they are interpretable in terms of the cluster model, suggest the existence of a cluster (^{3}He or ^{3}H) spin-orbit potential.

The presence of a spin-orbit potential pushes the $\frac{9}{2}^-$ cluster state in Fig. 12 to a very high energy in the continuum, so it should not be seen in the three particle transfer reaction. Indeed, it is very significant that the (nnp) transfer reaction[1] populates only the $\frac{11}{2}^-$ state at 13.15 MeV in ^{15}N and *not* the $\frac{9}{2}^-$ state at 11.94 MeV, although both states are seen strongly in two particle (np) transfer on a ^{13}C target.[43,44] It was precisely this type of observation that led to the $\frac{11}{2}^-$ and $\frac{13}{2}^+$ assignments for the 12.89 and 15.36 MeV states, respectively, seen in the ^{12}C(^{12}C, ^{9}Be)^{15}O reaction at 114 MeV.[2] The analog of the 12.89 MeV state lies at 13.15 MeV in ^{15}N and is strongly populated in (np) transfer. However, (np) transfer on ^{13}C could not populate the $[(d_{5/2})^2_{5+} \otimes d_{3/2}]_{13/2+}$ state, since one particle is in the $1p_{1/2}$ shell in the ^{13}C target. Assuming the (np) pair to be transferred as $(d_{5/2})^2_{5+}$, the spectator $1p_{1/2}$ particle of ^{13}C can couple to give $\frac{9}{2}^-$ or $\frac{11}{2}^-$ states, as observed. On the other hand, when three particles are transferred [(nnp) or (npp)], the cluster picture suggests maximum angular momentum transfer consistent with the assigned shell-model orbitals, i.e., $[(1d_{5/2})^2_{5+} \otimes 1p_{1/2}]_{11/2-}$ and $[(1d_{5/2})^2_{5+} \otimes 1d_{3/2}]_{13/2+}$. Thus both (np) and (nnp) transfer each give two strong peaks, but only one ($\frac{11}{2}^-$) in common.

To develop this line of reasoning further, we need to understand why the configuration $[(1d_{5/2})^2_{5+} \otimes 1p_{1/2}]_{11/2-}$ is likely to have large overlap with a triton cluster wave function and why $[(1d_{5/2})^2_{5+} \otimes 1p_{1/2}]_{9/2-}$ does not. In the L-S vector coupling picture, the $\frac{11}{2}^-$ state corresponds to $L=5$, $S=\frac{1}{2}$, which is suitable for a triton cluster. The $\frac{9}{2}^-$ state, on the other hand, arises from $L=3$, $S=\frac{3}{2}$. Since $S=\frac{3}{2}$ is ruled out for a triton cluster, the $[(1d_{5/2})^2_{5+} \otimes 1p_{1/2}]_{9/2-}$ configuration, corresponding to the $\frac{9}{2}^-$ state at 11.94 MeV in ^{15}N, should have negligible overlap with the $\frac{9}{2}^-$ cluster state. We suggest instead that the $[(1d_{5/2})^2_{4+,T=1} \otimes 1p_{1/2}]_{9/2-}$ configuration has strong overlap with the $\frac{9}{2}^-$ cluster state. Such a state would lie higher in energy and be very weakly excited in (np) transfer; indeed, there is no experimental evidence for $T=1$ (np) transfer. Finally, we observe that the

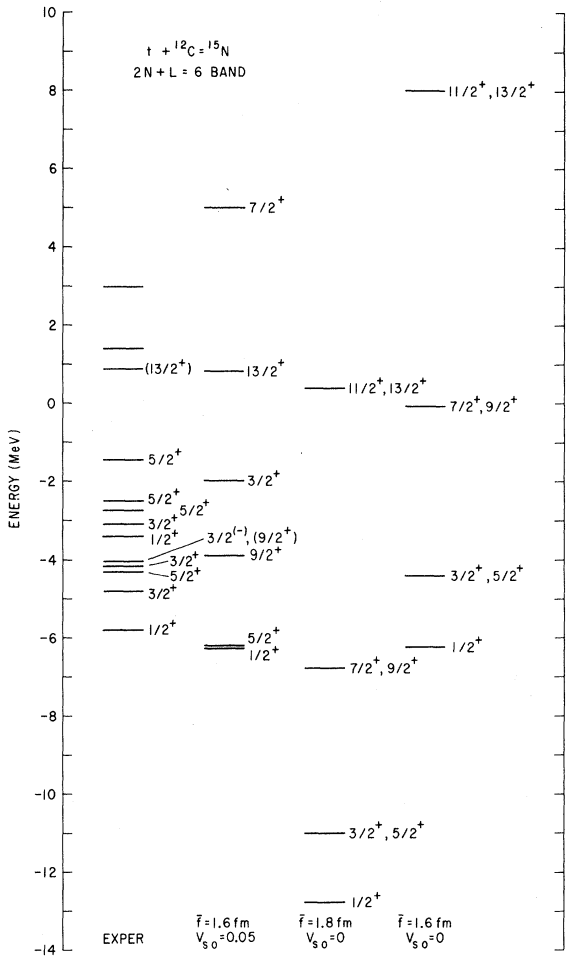

FIG. 13. Spectra for ^{3}H + ^{12}C cluster states in ^{15}N, corresponding to the $2N+L=6$ band. Experimentally observed positive parity states in the relevant energy region are also shown (Ref. 49). The highest two states, of unknown spin and parity, are seen fairly strongly in the ^{12}C(^{10}B, ^{7}Be)^{15}N reaction (Ref. 1), so we include them here. We have omitted the seven lowest positive parity states in ^{15}N ($\frac{5}{2}^+$, $\frac{1}{2}^+$, $\frac{5}{2}^+$, $\frac{3}{2}^+$, $\frac{7}{2}^+$, $\frac{1}{2}^+$, $\frac{3}{2}^+$) since these states are thought to correspond to the various couplings of two $1p_{1/2}$ particles and one $2s_{1/2}$ or $1d_{5/2}$ particle in the shell model (Ref. 51); they would hence have greater overlap with the $2N+L=4$ band than with the $2N+L=6$ band. The second column corresponds to a choice of $\bar{f}$ and V_{so} which fits the absolute energy of the assumed $\frac{13}{2}^+$ and $\frac{9}{2}^+$ states. Typical spectra obtained without a spin-orbit potential are shown in the last two columns.

configuration $(1d_{5/2})^2_{4+,T=1}$ is seen as a prominent peak in the (nn) or (pp) transfer on ^{12}C, leading to ^{14}C or ^{14}O.[43,50] The analog of this configuration in ^{14}N lies much higher in energy than the well-known $(1d_{5/2})^2_{5+,T=0}$ configuration. This lends support to the suggestion that the main configuration corresponding to the $\frac{9}{2}^-$ triton cluster state is $[(1d_{5/2})^2_{4+,T=1} \otimes 1p_{1/2}]_{9/2-}$. In conclusion, we regard the fact that the $\frac{9}{2}^-$ state at 11.94 MeV is *not* observed in (nnp) transfer on ^{12}C as one of the strongest supports for the whole idea of triton clusters.

Typical spectra for the $2N+L=6$ band in ^{15}N are shown in Fig. 13, together with experimentally observed positive parity states in the appropriate energy region.[49] In column 2 of Fig. 13, we show a spectrum obtained by adjusting V_{so} and $\bar{f}$ to produce the correct absolute energy and splitting for the $\frac{9}{2}^+$ and $\frac{13}{2}^+$ members of the band, assuming these states are to be identified with strong peaks seen in the ^{12}C(^{10}B, ^{7}Be)^{15}N reaction[1] at 10.8 and 15.7 MeV, respectively. A spin-orbit strength $V_{so}=0.05$ was required, which is the *same* value needed for the $2N+L=5$ band (see Fig. 12). In this case, the $\frac{1}{2}^+$, $\frac{3}{2}^+$, and $\frac{5}{2}^+$ members of the band also lie in an energy region where a number of states of the same spin and parity are found. However, for these relatively low-spin states, we do not expect the cluster strength to reside in only one experimental state. Hence, we do not pursue any more detailed attempt at identifying experimental and theoretical states. In columns 3 and 4 of Fig. 13, we show two spectra obtained without a spin-orbit potential. As for the $2N+L=5$ band, the theoretical spectrum is then far too spread out in energy; in particular the $\frac{9}{2}^+$-$\frac{13}{2}^+$ splitting is about 3 MeV too large. So we conclude again that a spin-orbit potential is necessary if we are to exhibit a sensible correspondence of existing data and theory.

The shell-model $[(d_{5/2})^2_{5+} \otimes d_{3/2}]_{13/2+}$ state lies in the region of 13–15 MeV, and presumably has strong overlap with the cluster model. The $\frac{9}{2}^+$ shell-model state lies several MeV lower in energy and is a mixture of the $(1d_{5/2})^3_{9/2+}$ and $[(1d_{5/2})^2 2s_{1/2}]_{9/2+}$ configurations[51]; hence, it could easily have a significant overlap with our postulated $2N+L=6$ triton structure. It should be noted that a well established[45] spin $\frac{3}{2}$ state lies at practically the same energy (10.8 MeV) as our suggested $\frac{9}{2}^+$ cluster state. However, it is kinematically very unlikely that a $\frac{3}{2}^{(-)}$ state would be strongly excited in heavy ion transfer reactions at high energies, for example ^{12}C(^{10}B, ^{7}Be)^{15}N at 100 MeV[1] or ^{12}C(^{12}C, ^{9}Be)^{15}O at 114 MeV.[2] On the other hand, a high-spin state such as $\frac{9}{2}^+$ would not have been seen in the ^{13}C(^{3}He,$p\gamma$)^{15}N reaction,[45] which was used to establish the $\frac{3}{2}^{(-)}$ state.

To summarize, we believe that the cluster model for ^{15}N is sensible for the $\frac{7}{2}^-$ and $\frac{11}{2}^-$ members of the $2N+L=5$ band and the $\frac{9}{2}^+$ and $\frac{13}{2}^+$ states in the $2N+L=6$ band. The model also predicts states of lower spin which are not in conflict with the observed spectrum. The spin assignments for these high-spin states are consistent with those based on purely kinematical considerations.[7] The depth parameter $\bar{f}$ of the folded cluster potential is consistent with that required for the discussion of α cluster states in Sec. III. In addition, our considerations suggest a cluster spin-orbit potential of the correct sign and magnitude, roughly consistent with that used for the description of the elastic scattering and polarization of tritons by nuclei.[52] On the whole, our interpretation of cluster states in ^{15}N is far less detailed and convincing than for the α-cluster states in ^{16}O and ^{20}Ne. One would expect that triton clusters are not as stable as α clusters under the influence of residual interactions. However, our model does predict large spectroscopic factors for triton cluster transfer to a certain restricted class of nuclear states. Detailed reaction theory calculations are required to test this hypothesis. Such calculations will be presented in a subsequent paper.[46]

---

*Work supported in part by the U. S. Atomic Energy Commission.

†This work was initiated while B. Buck was a summer visitor at Brookhaven National Laboratory in July, 1973.

[1]K. Nagatani, D. H. Youngblood, R. Kenefick, and J. Bronson, Phys. Rev. Lett. 31, 250 (1973).

[2]D. K. Scott, P. N. Hudson, P. S. Fisher, C. U. Cardinal, N. Anyas-Weiss, A. D. Panagiotou, P. J. Ellis, and B. Buck, Phys. Rev. Lett. 28, 2659 (1972); H. G. Bingham, M. L. Halbert, D. C. Hensley, E. Newman, K. Kemper, and R. White, unpublished.

[3]K. Bethge, Annu. Rev. Nucl. Sci. 20, 255 (1970). This is a good review article on α-transfer reactions which contains many references to earlier work; see also A. Arima, V. Gillet, and J. Ginocchio, Phys. Rev. Lett. 25, 1043 (1970).

[4]H. H. Gutbrod, H. Yoshida, and R. Bock, Nucl. Phys. A165, 240 (1971); M. Cobern, Ph.D. thesis, Yale University, 1974 (unpublished).

[5]J. D. Garrett, Argonne Informal Report No. PHY-1972H (unpublished), p. 232; see also contribution by H. T. Fortune to this report.

[6]R. M. DeVries, Nucl. Phys. A212, 207 (1973); J. Draayer, unpublished.

[7]D. M. Brink, Phys. Lett. 40B, 37 (1972).

[8]D. K. Scott, P. N. Hudson, P. S. Fisher, N. Anyas-Weiss, A. D. Panagiotou, and D. M. Brink, J. Phys. (Paris) 33, C5-58 (1972).
[9]D. M. Brink, in *Proceedings of the International School of Physics "Enrico Fermi," Course XXXVI, 1965,* edited by C. Bloch (Academic, New York, 1966), p. 247.
[10]J. P. Elliott, Proc. Roy. Soc. Lond. A245, 128, 562 (1958).
[11]M. Harvey, in *Advances in Nuclear Physics,* edited by M. Baranger and E. Vogt (Plenum, New York, 1968), Vol. 1, p. 67.
[12]H. R. Collard and R. Hofstadter, in *Landolt-Börnstein: Numerical Data and Functional Relationships in Science and Technology,* edited by K. H. Hellwege and H. Schopper (Springer-Verlag, Berlin, 1967), Group I, Vol. 2, p. 21.
[13]J. P. Vary and C. B. Dover, Phys. Rev. Lett. 31, 1510 (1973).
[14]Other versions of the folding model for α scattering have been considered by A. M. Bernstein and W. A. Seidler, Phys. Lett. 34B, 569 (1971); R. S. MackIntosh, Nucl. Phys. A210, 245 (1973); P. Mailandt, J. S. Lilley, and G. W. Greenlees, Phys. Rev. C 8, 2189 (1973); L. West, S. Cotanch, and D. Robson, in *Proceedings of the International Conference on Nuclear Physics, Munich, 1973,* edited by J. de Boer and H. J. Mang (North-Holland, Amsterdam/American Elsevier, N. Y., 1973), Vol. 1, p. 383.
[15]C. B. Dover and J. P. Vary, in Proceedings of the Heidelberg Symposium on Classical and Quantum Mechanical Aspects of Heavy Ion Collisions, October, 1974 (Springer-Verlag, to be published); BNL Report No. BNL 19332; J. P. Vary and C. B. Dover, in Proceedings of the Berkeley-Bevalac Heavy Ion Summer Study, 13–24 July 1974 (unpublished); BNL Report No. BNL 19360.
[16]A. Arima, H. Horiuchi, K. Kubodera, and N. Takigawa, in *Advances in Nuclear Physics,* edited by M. Baranger and E. Vogt (Plenum, New York, 1972), Vol. 5, p. 345. This comprehensive review article may be consulted for many references to earlier work on cluster models and a discussion of their foundations. For an even more extensive treatment, see K. Wildermuth and W. McClure, in *Springer Tracts in Modern Physics,* edited by G. Höhlen (Springer, New York, 1966), Vol. 41.
[17]A. Arima and S. Yoshida, Phys. Lett. 40B, 15 (1972).
[18]C. A. Mosley and H. T. Fortune, Phys. Rev. C 9, 775 (1974).
[19]A. Arima and S. Yoshida, Nucl. Phys. A219, 475 (1974).
[20]H. Horiuchi and K. Ikeda, Prog. Theor. Phys. 40, 277 (1968).
[21]J. Hiura, Y. Abe, S. Saito, and O. Endo, Prog. Theor. Phys. 42, 555 (1969).
[22]H. Horiuchi and Y. Suzuki, Prog. Theor. Phys. 49, 1974 (1973).
[23]T. Matsuse and M. Kamimura, Prog. Theor. Phys. 49, 1765 (1973).
[24]Y. Akiyama, A. Arima, and T. Sebe, Nucl. Phys. A138, 273 (1969); J. B. McGrory and B. H. Wildenthal, Phys. Rev. C 7, 974 (1973).
[25]E. C. Halbert, J. B. McGrory, and B. H. Wildenthal, Phys. Rev. Lett. 20, 1112 (1968).
[26]K. R. Lassey, M. R. P. Manning, and A. B. Volkov, Can. J. Phys. 51, 2522 (1973).
[27]F. Ajzenberg-Selove, Nucl. Phys. A190, 1 (1972).
[28]H. D. Lee and R. Y. Cusson, Ann. Phys. (N.Y.) 72, 353 (1972).
[29]G. Ripka, in *Advances in Nuclear Physics,* edited by M. Baranger and E. Vogt (see Ref. 11), Vol. 1.
[30]T. Une, Prog. Theor. Phys. 49, 1587 (1973).
[31]J. B. McGrory, Phys. Lett. 47B, 481 (1973).
[32]B. F. Bayman and A. Bohr, Nucl. Phys. 9, 596 (1959).
[33]A. M. Lane and R. G. Thomas, Rev. Mod. Phys. 30, 257 (1958).
[34]K. Yasaki, Prog. Theor. Phys. 49, 1205 (1973).
[35]O. Häusser, A. J. Ferguson, A. B. McDonald, I. M. Szöghy, T. K. Alexander, and D. L. Disdier, Nucl. Phys. A179, 465 (1972).
[36]T. K. Alexander, O. Häusser, A. B. McDonald, A. J. Ferguson, W. T. Diamond, and A. E. Litherland, Nucl. Phys. A179, 477 (1972).
[37]H. T. Fortune, R. R. Betts, J. D. Garrett, and R. Middleton, Phys. Lett. 44B, 65 (1973).
[38]L. R. B. Elton, *Nuclear Sizes* (Oxford U. P., Oxford, 1961).
[39]G. Bassani *et al.*, J. Phys. (Paris) 32, C6-133 (1971).
[40]V. I. Chuev *et al.*, J. Phys. (Paris) 32, C6-165 (1971).
[41]C. H. Holbrow, H. T. Fortune, and J. Garrett, Bull. Am. Phys. Soc. 19, 432 (1974).
[42]G. A. Norton, K. W. Kemper, G. E. Moore, R. J. Puigh, R. L. White, and M. E. Williams, Bull. Am. Phys. Soc. 19, 433 (1974).
[43]N. Anyas-Weiss, J. C. Cornell, P. S. Fisher, P. N. Hudson, A. Mechaca-Rocha, D. J. Millener, A. D. Panagiotou, D. K. Scott, D. Strottman, D. M. Brink, B. Buck, P. J. Ellis, and T. Engeland, Phys. Rep. 12C, 201 (1974).
[44]C. C. Lu, M. S. Zisman, and B. G. Harvey, Phys. Rev. 186, 1086 (1969).
[45]E. Warburton and J. Olness, Phys. Rev. 147, 698 (1966).
[46]C. B. Dover and J. P. Vary, unpublished.
[47]I. Rotter, Nucl. Phys. A135, 378 (1969).
[48]We would like to thank E. Auerbach for providing both the bound state and scattering versions of ABACUS.
[49]F. Ajzenberg-Selove, Nucl. Phys. A152, 1 (1970).
[50]J. H. Towle and G. J. Wall, Nucl. Phys. A118, 500 (1968).
[51]A. P. Zuker, B. Buck, and J. B. McGrory, BNL Report No. BNL 14085, 1969 (unpublished).
[52]R. L. Jutson *et al.*, Phys. Lett. 27B, 153 (1968); J. E. Engeland *et al.*, *ibid.* 30B, 476 (1969); T. F. Smith and P. D. Kunz, Bull. Am. Phys. Soc. 12, 1173 (1967).
[53]P. M. Endt and C. van der Leun, Nucl. Phys. A235, 27 (1974); J. D. Larson and R. H. Spear, *ibid.* 56, 497 (1964).
[54]S. Saito, Prog. Theor. Phys. 41, 705 (1969).
[55]T. Matsuse and M. Kamimura, Prog. Theor. Phys. 51, 438 (1974).
[56]A. P. Zuker, B. Buck, and J. B. McGrory, Phys. Rev. Lett. 21, 39 (1968).
[57]B. Buck, in Proceedings of the Heidelberg Symposium on Classical and Quantum Mechanical Aspects of Heavy Ion Collisions, October 1974 (see Ref. 15).
[58]G. R. Satchler, in *Proceedings of the International*

Conference on Reactions Between Complex Nuclei, Nashville, Tennessee, June 1974, edited by R. L. Robinson, F. K. McGowan, J. B. Ball, and J. H. Hamilton (North-Holland, Amsterdam/American Elsevier, New York, 1974).

[59]B. S. Reehal and B. H. Wildenthal, Particles and Nuclei 6, 137 (1973).